Supplementary Information: An Open Quantum Systems approach to proton tunnelling in DNA

Louie Slocombe*
Leverhulme Quantum Biology Doctoral Training Centre, University of Surrey, Guildford, GU2 7XH, UK.

Marco Sacchi†
Department of Chemistry, University of Surrey, Guildford, GU2 7XH, UK.

Jim Al-Khalili‡
Department of Physics, University of Surrey, Guildford, GU2 7XH, UK.

This material contains supplemental information for the results presented in the manuscript *An Open Quantum Systems approach to proton tunnelling in DNA*. In this file, unless otherwise stated, we use the Hartree atomic unit system, energy is in units of Hartrees E_h, the reduced Planck constant is $\hbar = 1$, and lengths are in Bohr radius a_0.

CONTENTS

* l.slocombe@surrey.ac.uk
† m.sacchi@surrey.ac.uk
‡ J.Al-Khalili@surrey.ac.uk

SUPPLEMENTARY NOTE 1: THE WIGNER-MOYAL CALDEIRA-LEGGETT MODEL

Wigner introduced a quantum-mechanical distribution function in phase space by considering the integral transform of the wave function [1]

$$W(q,p,t) = \frac{1}{\pi\hbar}\int \psi^*(q+q')\psi(q-q')e^{2ipq'/\hbar}dq', \tag{1}$$

or, for a mixed quantum state, using a density matrix,

$$W(q,p,t) = \frac{1}{2\pi\hbar}\int e^{-ipq'/\hbar}\left\langle q+\frac{q'}{2}\middle|\,\tilde{\rho}\,\middle|q-\frac{q'}{2}\right\rangle dq'. \tag{2}$$

The Wigner transformation is the Fourier transform of the antidiagonals of the density matrix when that matrix is expressed in the position basis. Taking the partial time derivative and employing the time-dependent Schrödinger equation, we obtain the Wigner-Moyal (WM) equation describing the time evolution of the Wigner function. Explicitly:

$$\frac{\partial}{\partial t}W(q,p,t) = -\mathcal{L}(q,p)\,W(q,p,t). \tag{3}$$

The WM equation is a deterministic dynamical equation that encapsulates the uncertainty in position q and momentum p into a quasi-probability density $W(q,p,t)$ [1, 2]. The quantum Liouvillian ($\mathcal{L}$) for the Wigner function is given by the kinetic ($\mathcal{K}$) and potential ($\mathcal{V}$) terms

$$\mathcal{L}(q,p) \equiv \mathcal{K}(q,p) + \mathcal{V}(q,p). \tag{4}$$

with terms,

$$\mathcal{K}(q,p)W(q,p) \equiv \frac{p}{m}\frac{\partial}{\partial q}W(q,p) \tag{5}$$

and

$$\mathcal{V}(q,p)W(q,p) \equiv \frac{i}{\hbar}\left(\mathcal{V}(q)\star W(p,q) - W(p,q)\star\mathcal{V}(q)\right). \tag{6}$$

Here, we use the star operator, $\star$, corresponding to the Moyal product [3, 4],

$$\star \equiv \exp\left[\frac{i}{2}\left(\underset{\leftarrow_q}{\partial}\underset{\rightarrow_p}{\partial} - \underset{\rightarrow_q}{\partial}\underset{\leftarrow_p}{\partial}\right)\right]. \tag{7}$$

The directional differentiation operators from the left and right appearing here are defined as

$$\underset{\rightarrow_x}{\partial} f(x) = f(x)\underset{\leftarrow_x}{\partial} \equiv \frac{\partial f(x)}{\partial x}. \tag{8}$$

For brevity we drop the dependence and expand the potential terms,

$$\frac{\partial W}{\partial t} = -\frac{p}{m}\frac{\partial W}{\partial q} + \frac{\partial V}{\partial q}\frac{\partial W}{\partial p} - \frac{\hbar^2}{24}\frac{\partial^3 V}{\partial q^3}\frac{\partial^3 W}{\partial p^3} + \mathcal{O}\left(\hbar^4\right). \tag{9}$$

Here the potential terms have been expanded as the Taylor series truncated to just the first two terms, which is frequently done in literature [2]. The series expansion contains powers of $\hbar$ and introduces quantum effects into the dynamics. The equivalent phase-space formulation of Caldeira-Leggett's model, also known as the Wigner-Moyal Caldeira-Leggett (WM-CL) equation, is written as [1, 5]

$$\frac{\partial W}{\partial t} = \underbrace{-\frac{p}{m}\frac{\partial W}{\partial q} + \frac{\partial V}{\partial q}\frac{\partial W}{\partial p} - \frac{\hbar^2}{24}\frac{\partial^3 V}{\partial q^3}\frac{\partial^3 W}{\partial p^3} + \mathcal{O}\left(\hbar^4\right)}_{\text{Schrödinger dynamics}} \underbrace{+\gamma\frac{\partial pW}{\partial p}}_{\text{Dissipation}} \underbrace{+\gamma m k_{\mathrm{B}}T\frac{\partial^2 W}{\partial p^2}}_{\text{Decoherence}}. \tag{10}$$

The WM-CL equation has a similar form to the WM equation [6]; however, it now contains two additional terms describing dissipation and decoherence arising from the coupling to the quantum bath.

A. Properties

In general, the expectation value of an observable, $\hat{O}$, can be defined as

$$\langle \hat{O} \rangle = \int_{-\infty}^{\infty} \int_{-\infty}^{\infty} W(q,p,t)\, \hat{O}\, dq\, dp. \tag{11}$$

For example, the expectation values of the position and momentum are

$$\langle Q(t) \rangle = \int_{-\infty}^{\infty} \int_{-\infty}^{\infty} W(q,p,t)\, q\, dq\, dp \tag{12}$$

and

$$\langle P(t) \rangle = \int_{-\infty}^{\infty} \int_{-\infty}^{\infty} W(q,p,t)\, p\, dq\, dp. \tag{13}$$

The total energy expectation value is then

$$\langle E(t) \rangle = \int_{-\infty}^{\infty} \int_{-\infty}^{\infty} W(q,p,t) \left(\frac{p^2}{2m} + V(q) \right) dq\, dp. \tag{14}$$

If an OQS starts in a pure state, the bath's interactions will cause it to decohere, driving it to a mixed state [7]. The purity of a quantum system can be measured using [8]

$$\mathcal{P}(t) = 2\pi\hbar \int_{-\infty}^{\infty} \int_{-\infty}^{\infty} W^2(q,p,t)\, dq\, dp. \tag{15}$$

B. The Low-Temperature Correction

To extend the temperature limit, one can adopt an effective harmonic approach by keeping the coth term in the influence functional intact. The thermal energy can be replaced with the average thermal energy of the oscillator [9–13],

$$k_{\mathrm{B}}T \to E_\omega = \frac{\hbar\omega}{2} \coth\left(\frac{\hbar\omega}{2k_{\mathrm{B}}T} \right) \sim \beta^{-1}. \tag{16}$$

Here, ω corresponds to the spring constant that best approximates the system's zero-point energy. The above holds in the high-temperature limit where the leading order term of the Taylor series of coth can be safely adopted. The high-temperature limit can be relaxed by undoing the leading order coth approximation taken in the influence functional [5, 9–13]. Substituting this back in, the WM-CL now reads,

$$\frac{\partial W}{\partial t} = -\frac{p}{m}\frac{\partial W}{\partial q} + \frac{\partial V}{\partial q}\frac{\partial W}{\partial p} - \frac{\hbar^2}{24}\frac{\partial^3 V}{\partial q^3}\frac{\partial^3 W}{\partial p^3} + \gamma \frac{\partial p W}{\partial p} + \gamma m \frac{\hbar\omega}{2} \coth\left(\frac{\hbar\omega}{2k_{\mathrm{B}}T} \right) \frac{\partial^2 W}{\partial p^2}. \tag{17}$$

The modified master equation above implies no restriction on the ratio $k_{\mathrm{B}}T/E_0$ while still being limited to the weak-coupling regime. This method is more straightforward to apply and allows application into the low-temperature regime; however, it does not fix the positivity issues of the Caldeira-Leggett model.

C. The Thermal Solution

A system coupled to a bath will eventually reach a state of thermal equilibrium in which its eigenstates are populated according to a Maxwell-Boltzmann distribution, $W^{\mathrm{eq}}(q,p) = W(q,p,t \to \infty)$. In the high-temperature limit, the distribution reads [14, 15]

$$W^{\mathrm{eq}}(p,q) = \frac{1}{\mathcal{N}} \exp\left[-\beta\, \mathcal{H} \right] \tag{18}$$

$$= \frac{1}{\mathcal{N}} \exp\left[-\frac{1}{k_{\mathrm{B}}T} \left(\frac{p^2}{2m} + V(q) \right) \right], \tag{19}$$

where $\mathcal{N}$ is a normalisation constant, $\beta = 1/(k_{\mathrm{B}}T)$, and $\mathcal{H}$ is the total energy of the system, the sum of kinetic and potential energy, corresponding to the Hamiltonian $p^2/(2m) + V(q)$. Thus, the thermal solution provides an easy measure of the thermal properties of the distribution and a straightforward check of numerical models over long integration times.

However, in the low-temperature case, the stationary thermal solution is modified. The thermal distribution now takes the form [9–13]

$$W^{\mathrm{eq}}(p,q) = \frac{1}{\mathcal{N}} \exp\left[-\frac{\mathcal{H}}{E_\omega}\right], \tag{20}$$

which is valid at low temperatures [9]. The thermal solution now tends to the zero-point energy of the quantum system at low temperature while maintaining the same form as Supplementary Equation 18 at high temperatures.

SUPPLEMENTARY NOTE 2: EXAMINING THE LOW-TEMPERATURE CORRECTION

Here we examine the low-temperature correction and validate our computational implementation used to solve the CL equation in phase-space. We compare numerical results to the expected analytical solution for a particle in a harmonic well, both with the temperature corrections and without.

D. The Harmonic Potential Well

We define the harmonic well as:

$$V(q) = \frac{1}{2} m\omega^2 q^2, \tag{21}$$

where, m denotes the particle's mass, ω is the angular frequency of the oscillator, and q is the position coordinate in phase-space.

We will consider a proton, $m = 1836\,\mathrm{a.u.}$, in a harmonic potential well with $\omega = 0.005\,\mathrm{AUT}^{-1} = 1836\,\mathrm{ps}^{-1}$, see Supplementary Figure 1. This spring constant is chosen such that the zero-point energy is greater than the thermal energy at biological temperatures, ensuring that we encounter the temperature limit.

1. Analytical Solutions

Analytical solutions for the harmonic oscillator for both dissipative and non-dissipative systems are known and are well studied (see ref. [16] and references therein). In the case of an initial displacement of q_0, and no initial momentum, the expectation value is given by,

$$\langle Q(t)\rangle = q_0 \exp\left(-\frac{\gamma}{2}t\right)\left(\cos(\omega_1 t) + \frac{\gamma}{2\omega_1}\sin(\omega_1 t)\right). \tag{22}$$

With subterm, ω_1 which denotes the perturbed frequency,

$$\omega_1 = \sqrt{\omega^2 - \frac{\gamma^2}{4}}. \tag{23}$$

Here, γ is the damping constant (bath coupling constant). Likewise, the expectation value for the momentum reads,

$$\langle P(t)\rangle = -\frac{m\omega^2 q_0}{\omega_1} \exp\left(-\frac{\gamma}{2}t\right)\sin(\omega_1 t). \tag{24}$$

If we take $\gamma \to 0$, we recover the solutions of a harmonic oscillator in a closed system. Moreover, the vanishing of the exponential terms implies that the position and momentum continue to exchange without loss, creating a circular orbit in phase-space.

For the dissipative system, over time, the orbit never reaches its original starting position. Instead, it decays to the bottom of the well. After several intervals of γ, the distribution fully decays to the bottom of the well, and we reach

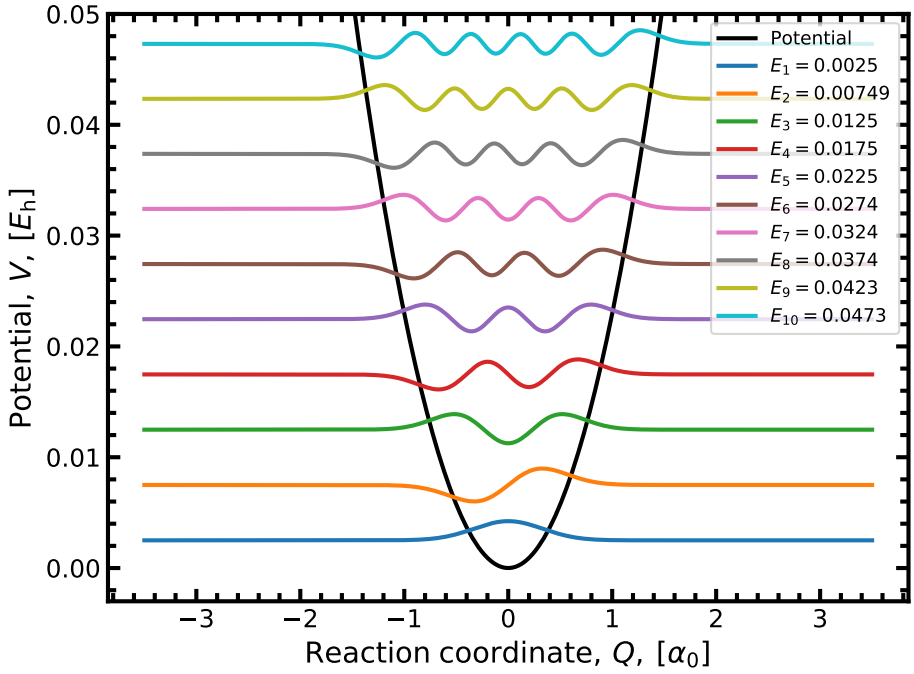

Supplementary Figure 1: A plot of the harmonic potential well with the first ten eigenstates plotted. The potential well parameters are picked the energy of the lowest oscillator is greater than the thermal energy, $E_0 > k_B T$. The lowest eigenstate has an energy of $0.0025\,E_h$ compared to the thermal energy of $0.000\,95\,E_h$ at 300 K.

a stationary state; we can also say that it is in thermal equilibrium with the bath. Here the variance is constant, defining the width of the distribution in phase-space. At equilibrium, the position variance is defined as [9, 16]

$$\langle Q^2 \rangle = \frac{\hbar}{2m\omega} \coth\left(\frac{\beta\hbar\omega}{2}\right) \sim \frac{1}{\beta m\omega^2}. \tag{25}$$

By expanding the coth term and approximating with the leading order term, we arrive at the high-temperature limit solution seen on the right-hand side of the equation. Likewise, the variance in momentum is defined as [13]

$$\langle P^2 \rangle = \frac{\hbar\omega m}{2} \coth\left(\frac{\beta\hbar\omega}{2}\right) \sim \frac{m}{\beta}. \tag{26}$$

Consequently, using these equations, we can validate our numerical solution at a given time using the expectation values and at $t \to \infty$ using the variances.

To compare analytical and numerical values, we use the L_2-norm, which measures the distance of the vector coordinate x_i from the origin of the vector space (or to some reference, r). It is defined as,

$$L_2\text{−norm} = \left(\sum_i |x_i - r|^2\right)^{1/2}. \tag{27}$$

2. Validating the Low-Temperature Correction

Now, we compare the solutions of a particle in a harmonic well in both the low and high-temperature expansions. At different temperatures, a Wigner distribution can be plotted using Supplementary Equation 20.

In order to verify the low-temperature method, we compare $k_B T$ directly to E_ω over a range of temperatures. If at the temperature of interest, we see a deviation between $k_B T$ and E_ω then it is not safe to truncate the coth term to the leading order. Hence, a low-temperature treatment is required for biological temperature.

Here, Supplementary Figure 2 describes a convincing narrative. At high temperatures, the thermal energy matches the coth result. However, at low temperature, the coth function levels out, tending asymptotically to temperature

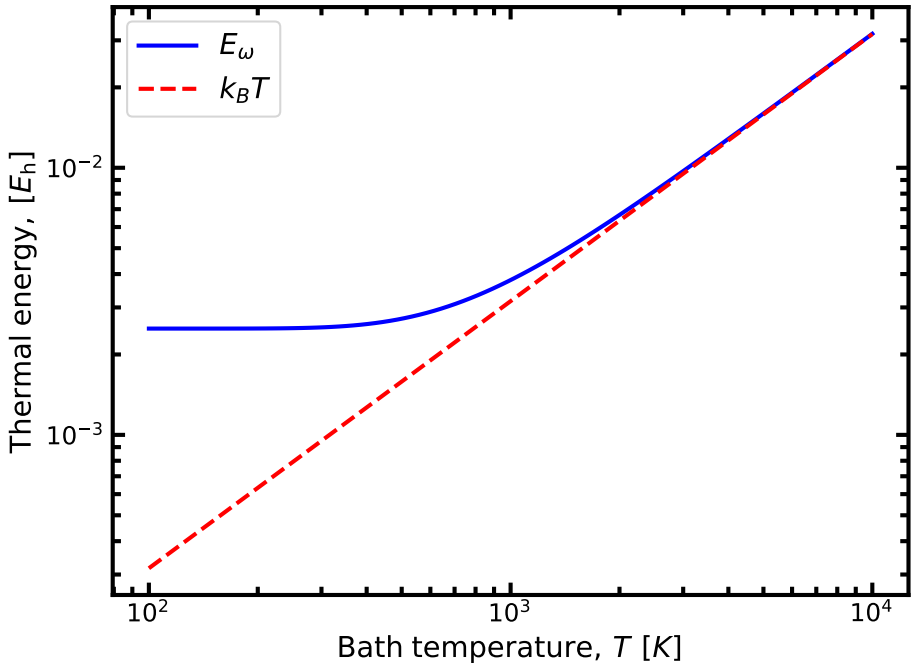

Supplementary Figure 2: The breakdown of the high-temperature limit by taking the leading order in β in comparison to the full coth solution, E_ω. It is clear that at biological temperatures, the treatments of the thermal energy significantly deviate.

independence, while the thermal energy continues its downward linear trend. The levelling off implies that the zero-point energy does not vanish, as one would expect for a quantum system.

The top panel in Supplementary Figure 3 demonstrates purity values greater than unity for the high-temperature approximation. The upper bound of this metric should saturate at unity since for a correctly normalised state, $\mathrm{Tr}\left(\hat{\rho}^2\right) = \mathrm{Tr}(\hat{\rho}) = 1$. A purity value greater than unity indicates the breakdown of decoherence using the high-temperature approximation, which diverges at low temperatures in an exponential fashion.

At the same time, the modified thermal energy approach suggests that deviation from a pure state (purity of unity) should tend to zero. The observed trend suggests that the bath has little impact on the system's coherence at low temperatures. Conversely, the two approaches tend to have a similar result at high temperatures: a low final coherence at thermal equilibrium.

The lower panel confirms that the two approaches compare at high temperatures as expected. While at low temperatures, the high-temperature approximation suggests that the thermal energy tends to zero, implying that the thermal equilibrium energy disappears. Nevertheless, traditional quantum mechanics suggests that at 0 K the system would still retain some energy - the zero-point energy. Therefore, as predicted in the low-temperature approximation, the non-zero minimum energy should tend to zero-point energy.

Supplementary Figure 4 demonstrates that the high-temperature limit fails to capture the minimal spread of the distribution. At low temperatures, both the Q and P variance tend to zero-indicating that the distribution becomes increasingly localised. Using atomic units $\hbar$ is unity, so the minimum uncertainty corresponds to 0.5 before the uncertainty principle is violated. Supplementary Figure 4 confirms that the low-temperature extension does not violate the uncertainty principle at low temperatures, whereas the high-temperature approximation does.

E. Numerical Calculations

Now let us consider a concrete numerical example in the harmonic well. As previously mentioned, at room temperature, the system's zero-point energy is much less than the thermal energy, $E_0 = 0.0025\,E_\mathrm{h}$ compared to $k_\mathrm{B}T = 0.000\,95\,E_\mathrm{h}$. Consequently, the temperature correction terms are required to model the system appropriately.

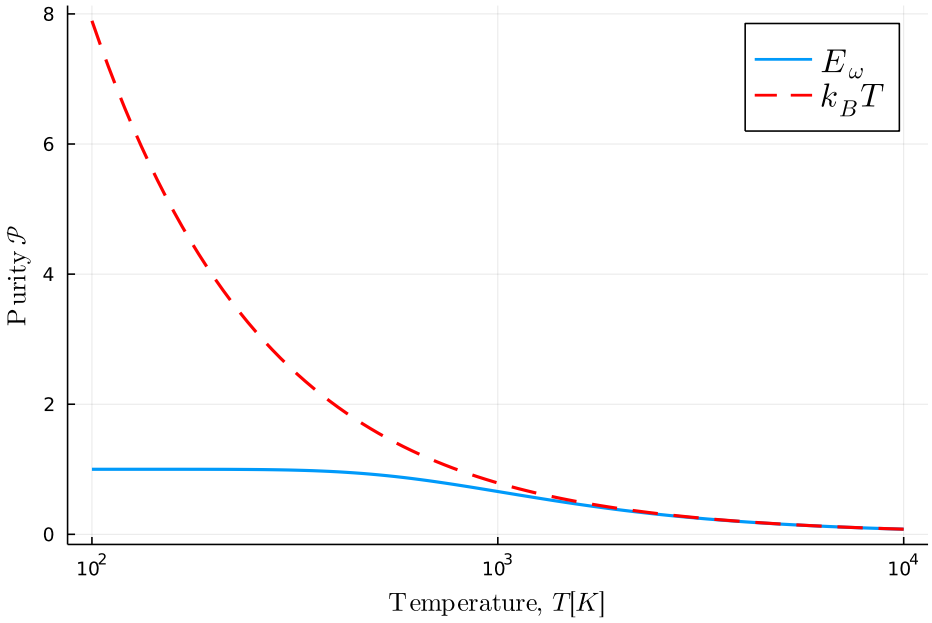

(a) Measuring the purity of the thermal solution

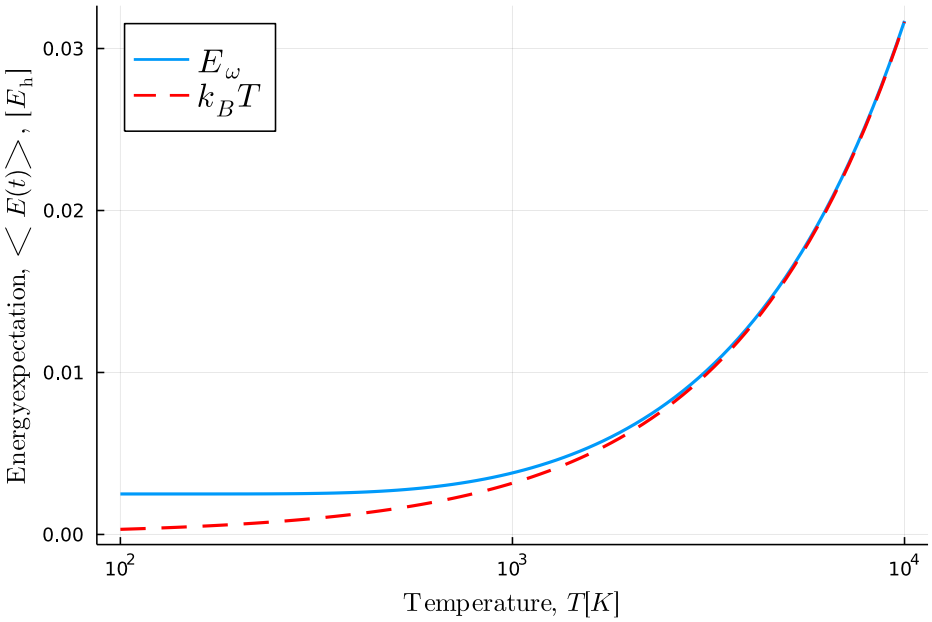

(b) The total energy expectation value of the thermal solution

Supplementary Figure 3: The purity and total energy expectation value at varying temperatures, calculated using Supplementary Equation 15 and Supplementary Equation 14. The high-temperature (dashed red line) approximation is compared to the low-temperature (solid blue line) approach.

We will consider an initial distribution given by a displaced thermal state (Supplementary Equation 28), [9]

$$W(x,p;t=0) = \frac{1}{\mathcal{N}} \exp\left(-\frac{2E_\omega}{\hbar^2}\left(m(q-q_0)^2 + \frac{1}{m\omega^2}(p-p_0)^2\right)\right) \tag{28}$$

Here, q_0, p_0 locate the position of the distribution maximum in phase space. While solving the WM-CL equation, we use a numerical grid of $N_q = N_p = 2^8$ elements, and with a solver tolerance (relative and absolute error) of 1×10^{-14} which corresponds to the machine precision of a 64-bit number.

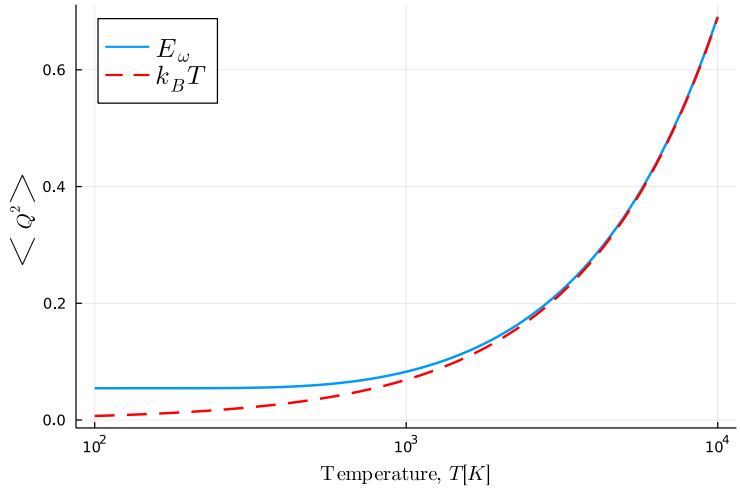

(a) Second moment of the position coordinate

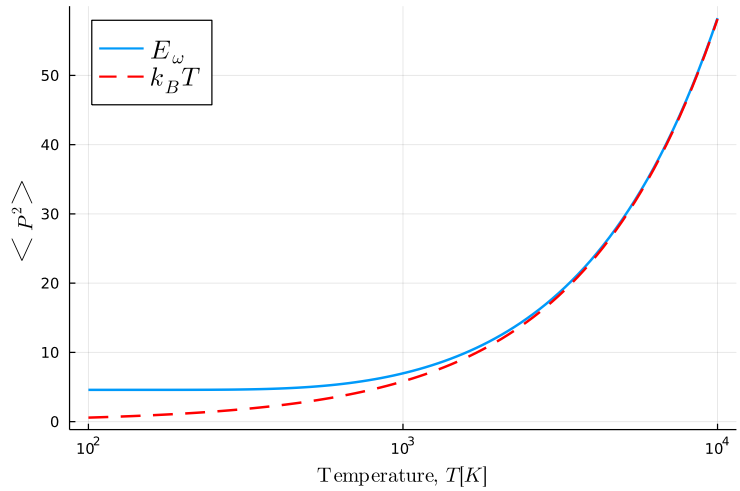

(b) Second moment of the momentum coordinate

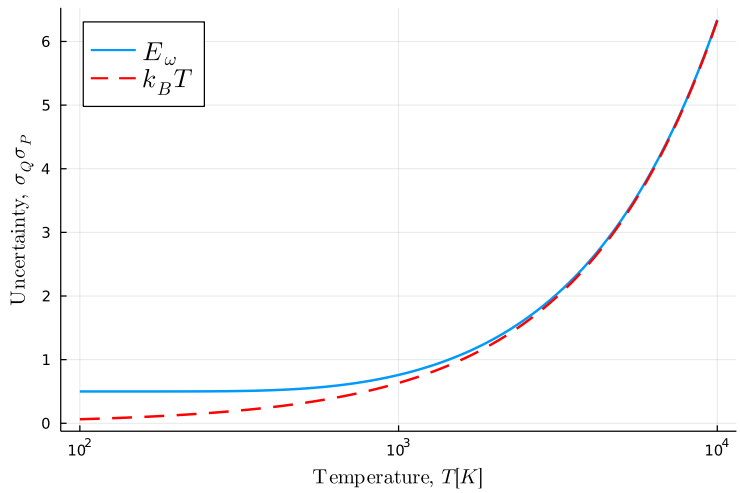

(c) Total energy expectation value

Supplementary Figure 4: Comparison of the position and momentum second moments, and the position-momentum uncertainty principle for the low and high-temperature treatments. At high temperatures, the two treatments converge. The high-temperature (dashed red line) approximation is compared to the low-temperature (solid blue line) approach.

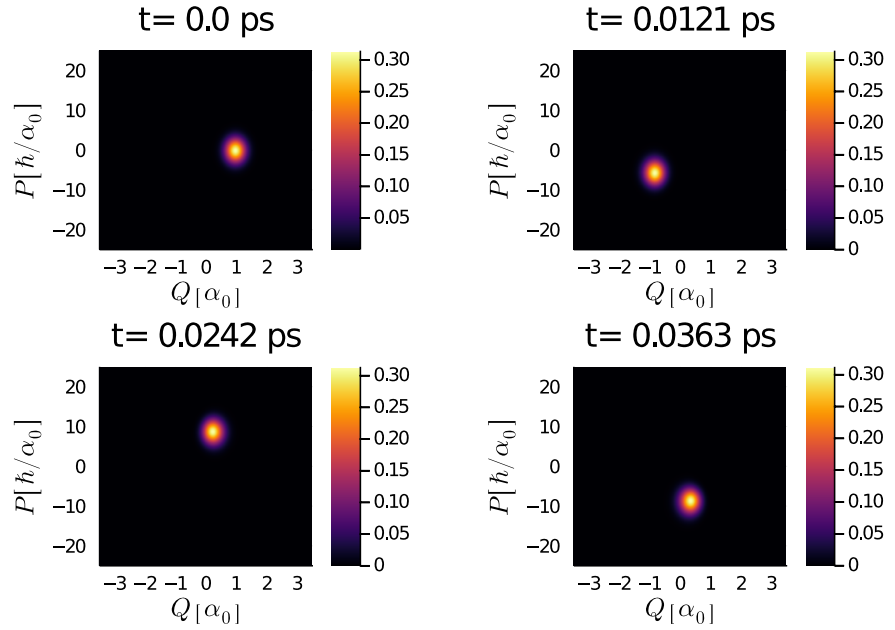

Supplementary Figure 5: Heatmap plots of the Wigner distribution at different times. Initially, the distribution is offset from the potential well minimum. Then, the distribution completes just over one orbit while oscillating around in a harmonic potential well.

For a closed quantum system, $\gamma = 0$, the exponential factors in Supplementary Equation 22 and 24 become unity and the sin term in Supplementary Equation 22 becomes zero. The distribution orbits around the origin in phase space, see Supplementary Figure 5. In Supplementary Figure 5 four heatmap plots are displayed, the timestamp of each plot is shown above. Initially, the distribution is centred at $q_0 = 1.0$ and $p_0 = 0.0$. However, as the system evolves, the distribution moves in a clockwise orbit in phase space. Consequently, $\langle Q(t) \rangle$ and $\langle P(t) \rangle$ are expected to loop around in phase-space as their values are conserved indefinitely. The result is a circle in phase-space, as shown in Supplementary Figure 6. Any deviation will be due to numerical dissipation only. Here, the numerical results directly overlay the analytical result. The deviation from the expectation values is shown in Supplementary Figure 7. For both cases, the l_2-norm errors are near machine precision.

We now turn our attention to the system when it is in contact with a bath. Like a classical oscillator, the dissipative case of a quantum harmonic oscillator has three regimes depending on the strength of the coupling to the environment: under-, critically, and over-damped. The underdamped case is demonstrated in Supplementary Figure 8 as the distribution slowly spirals in towards the bottom of the well. The deviation from the expectation values is shown in Supplementary Figure 8. While the thermal limit is breached, the distribution can maintain the position and momentum expectation values. However, as indicated by the top panel, the distribution's width is not correctly conserved; instead, the distribution tightens to a point-like state.

To further investigate the low-temperature corrections, we compare the energy expectation value, purity, and uncertainty principle for the low- and high-temperature approximation. We compare the observables to the value reported by the thermal solution given by Supplementary Equation 20. We repeat this for the WM-CL equation with and without the corrections.

The left-hand columns of Supplementary Figure 9 displays the observables for the uncorrected WM-CL equation. The top panel shows that the uncorrected WM-CL equation fails to match the low-temperature analytical solution. The purity rises to a maximum value that is greater than unity, which is unphysical. Furthermore, the system becomes point-like and violates the uncertainty principle. The values incorrectly equilibrate to the high-temperature limit of Supplementary Equation 20.

By comparison, the right-hand columns of Supplementary Figure 9 displays the low-temperature corrected WM-CL equation. The equation leads to the correct total energy - which corresponds to the low-temperature thermal solution. The purity now drops from the initial value of unity to near the thermal solution. However, the discrepancy can be removed by increasing the numerical grid size. Now the uncertainty principle tends to the correct value. The initial value is below the allowed value of 0.5, but it is attributed to numerical noise propagated to the double integrals in the width calculations. The discrepancy is controlled by the grid size and the solver tolerance.

Note that the initial y-axis values for all the panels are not the same; this is a consequence of taking Supplementary

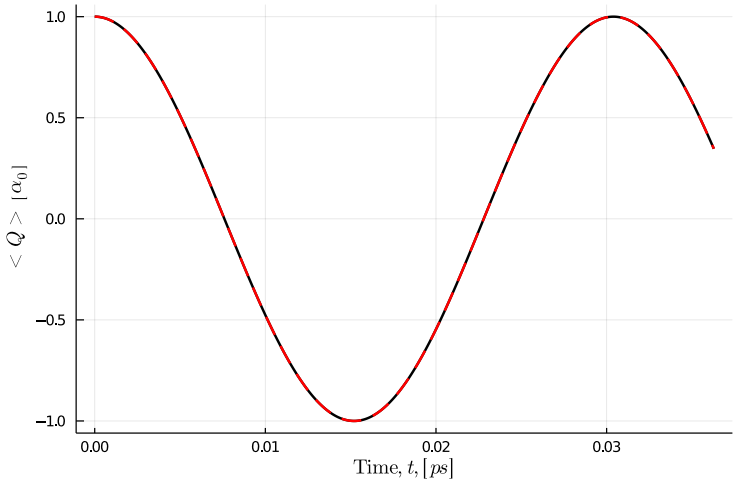

(a) Position expectation value

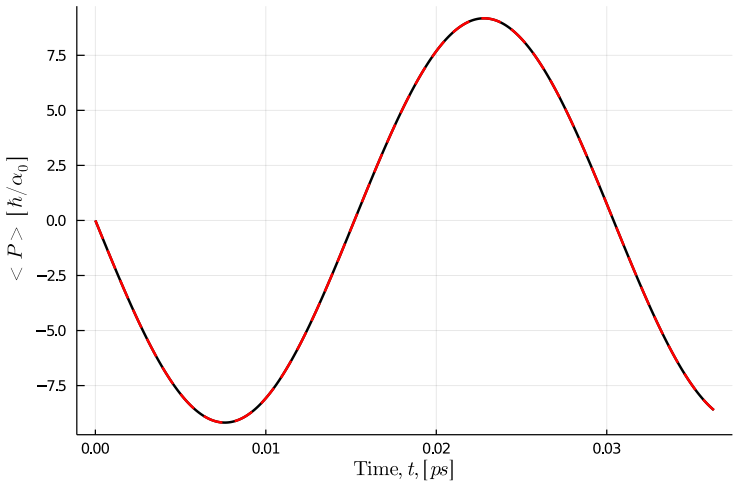

(b) Momentum expectation value

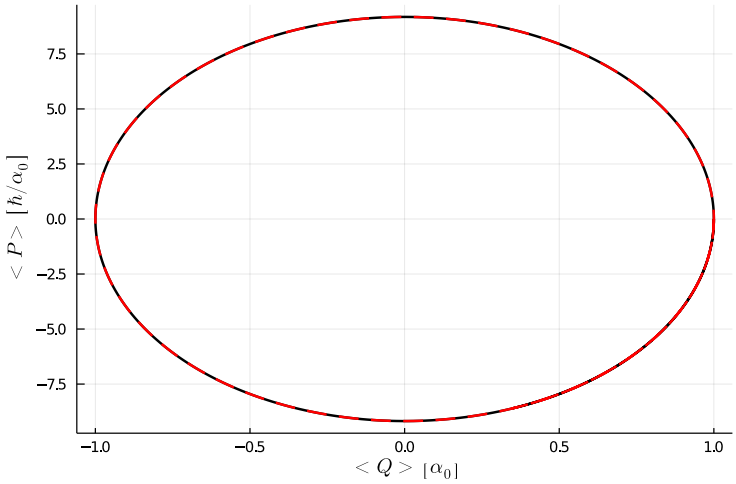

(c) Parametric plot of both expectation values

Supplementary Figure 6: (a-b) Initially, the distribution is centred at $q_0 = 1.0$ and $p_0 = 0.0$, the expectation values oscillate 90° out of phase of each other. On a parametric plot (c) of the expectation, values will oscillate indefinitely for a closed quantum system of a particle in a harmonic well. The numerical expectation values are plotted in black, and the red dotted line shows the analytical values. The numerical and analytical lines overlap so that the red line overlays the black.

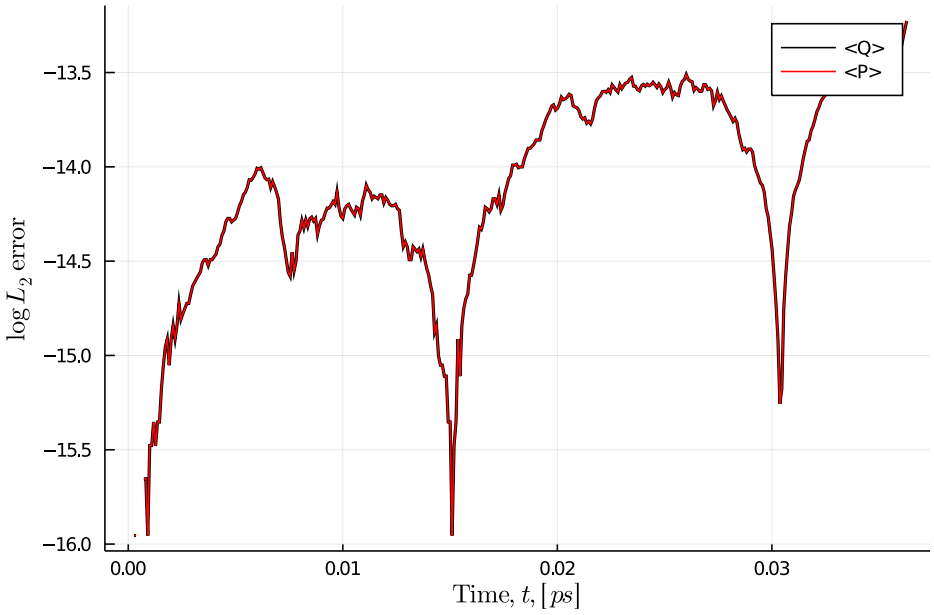

Supplementary Figure 7: L_2-norm error between the numerical and analytical expectation values for position and momentum. The position values are plotted in black, and the momentum values are in red. The errors are so small that they are comparable to the machine precision (1×10^{-16}). Furthermore, both lines strongly correlate and overlap such that only the red line is visible.

Equation 20 to the high and low-temperature limit, hence giving different values. In summary, the low-temperature corrected WM-CL equation provides adequate coverage for biological temperatures and can accurately reproduce analytical solutions of the finial thermal equilibrium.

SUPPLEMENTARY NOTE 3: TUNNELLING COMPARISON

First introduced by Topaler and Makri [17] the Double Well 1 potential is a benchmark that several authors have used for a comparison of tunnelling corrections [17–22]. We will use it to compare our numerical solutions to published results.

DW1 serves as a symmetric potential of moderate barrier height and well width. It has been studied using path integral methods [17] and polymer ring dynamics [18, 22]. In particular, we will compare our results to Craig *et al.* [18] who use this potential to study a proton transfer reaction in model condensed-phase environments. The model potential is given by

$$V(q) = \frac{m^2\omega_m^4}{64E_b}q^4 - \frac{m\omega_m^2}{4}q^2, \tag{29}$$

with mass $m = m_p$, a well barrier of $E_b = 2085\,\mathrm{cm}^{-1} = 0.009\,50\,E_\mathrm{h}$, and a frequency at the well minimum $\omega_m = 707\,\mathrm{cm}^{-1} = 0.003\,22\,\hbar/E_\mathrm{h}$. The DW1 potential with the first 6 eigenstates are shown in Supplementary Figure 10.

To achieve the quantum contributions to the chemical rate, we insert the DW1 potential into our system Hamiltonian. We then integrate the WM-CL equation to determine the quantum-to-classical ratio.

In Supplementary Figure 11 we compare the quantum-to-classical ratio of the rate for two cases of bath coupling, $\gamma = 0.05\omega_b$ and $\gamma = 0.95\omega_b$ where ω_b is the barrier spring constant.

At low coupling strengths, the process of energy dissipation imposed on the system by the bath is slow. Consequently, the system recrosses the transition state barrier several times before it stabilises, plateauing at a constant value. The recrossing of the barrier leads to the oscillatory structure seen in plot (a) of Supplementary Figure 11. Our result for κ is shown in (b) and only reaches a maximum that is about 50% of the Craig value. However, we observe a similar asymptotic value of $\kappa = 0.52$, which is 86% close to Craig.

On the other hand, for the high-friction case shown in (c) and (d) of Supplementary Figure 11; there is no recrossing after an initial spike. In this regime, the rate quickly rises over a range of 30 fs before decaying to a plateau value

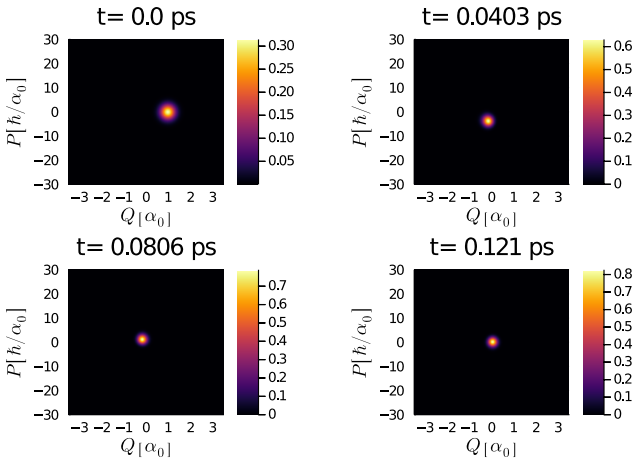

(a) Evolution of the Wigner-Moyal Caldeira–Leggett equation

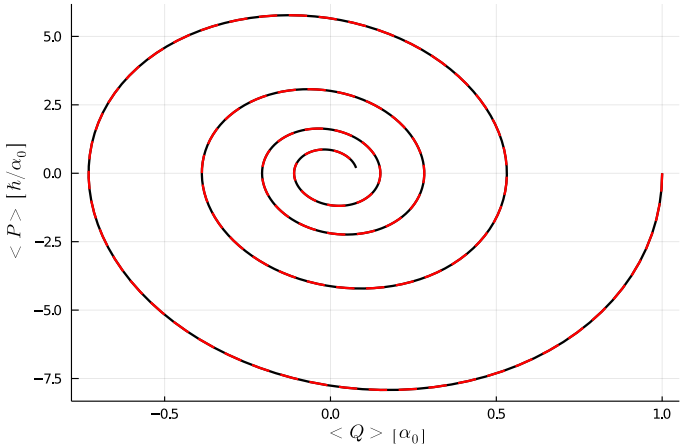

(b) Decay of the expectation values; momentum expectation value against the position value

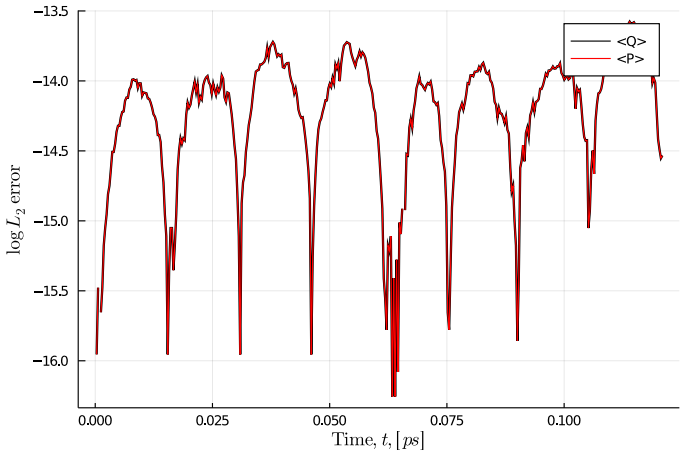

(c) L_2 error in the expectation values

Supplementary Figure 8: The expectation values will decay to a constant value for an open quantum system of a particle in a harmonic well. (a) Demonstrates the distribution contracting and falling to the bottom of the well. (b) The peak of the distribution in phase space (the expectation values) spirals towards the bottom of the well. The numerical expectation values are plotted in black, and the analytical solutions in dashed red. (c) The corresponding error of (b) oscillates by over two orders of magnitude. However, the numerical solutions for the expectation values match the analytical values near machine precision and do not grow exponentially, indicating little numerical dispersion.

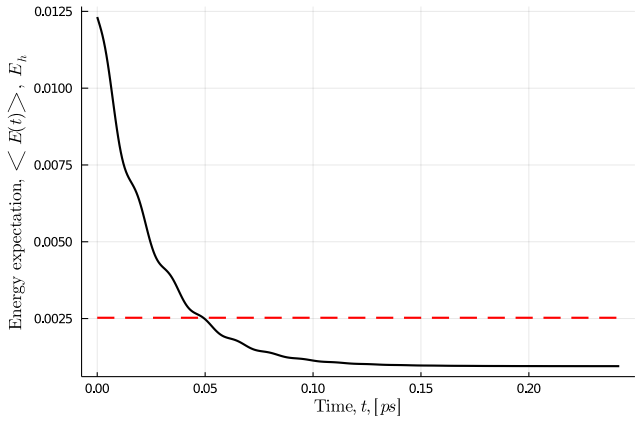

(a) Excessive decay of total energy expectation value

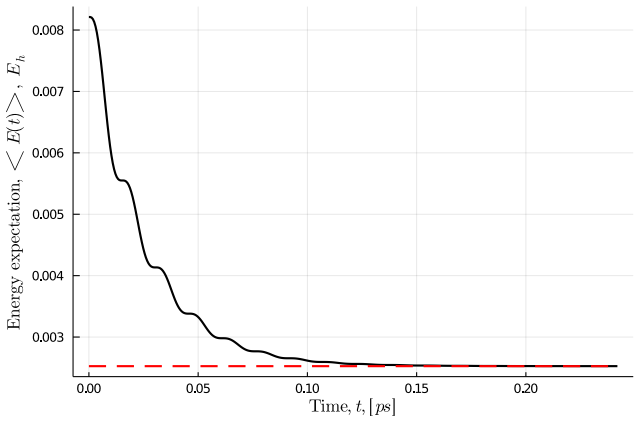

(b) Maintaining the total energy expectation value

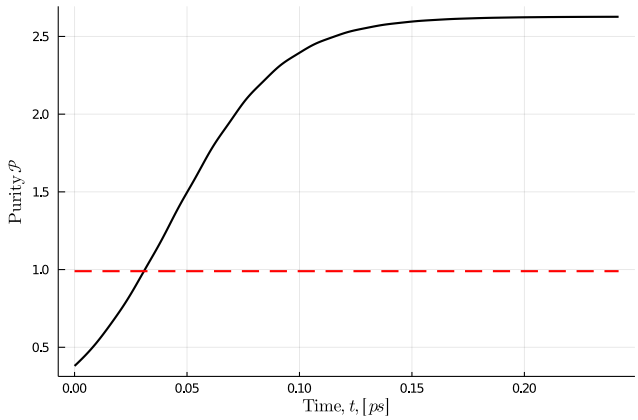

(c) Break down of decoherence

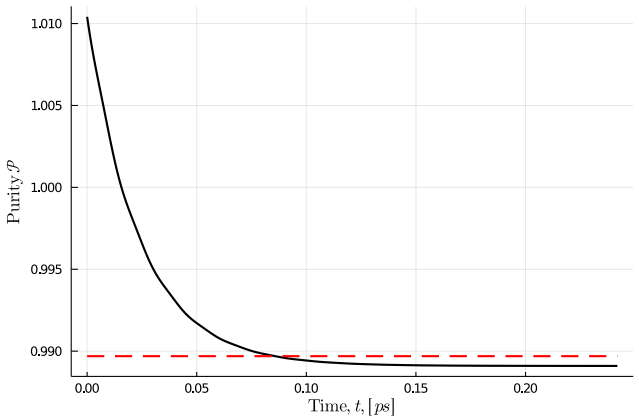

(d) Decoherence

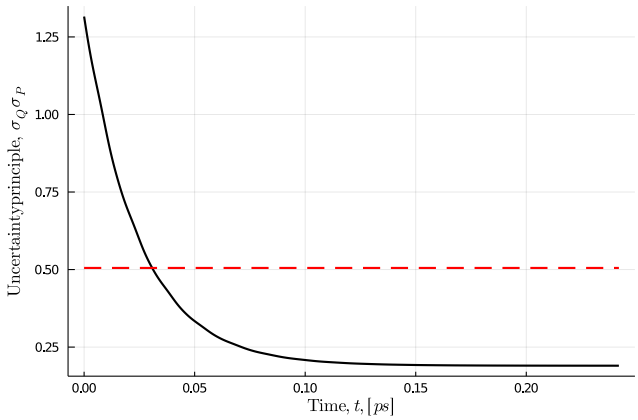

(e) Violation of the uncertainty principle

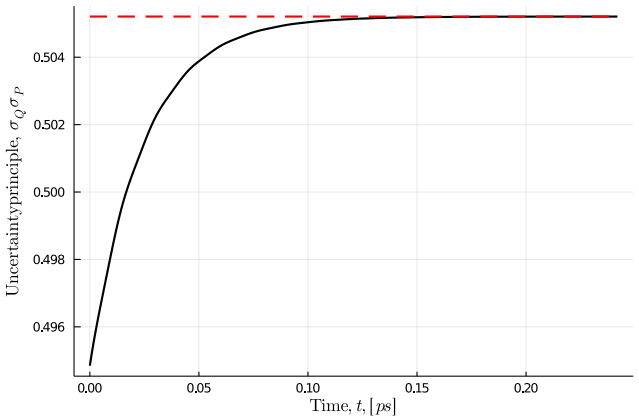

(f) Correct uncertainty

Supplementary Figure 9: Properties of the WM-CL in a harmonic well, the expected analytical thermal solution is plotted in a red dotted line. The left-hand column corresponds to the high-temperature WM-CL equation. In comparison, the right-hand column is the low-temperature corrected equation. The low-temperature corrected solutions correctly predict the analytical distribution properties when $t \to \infty$.

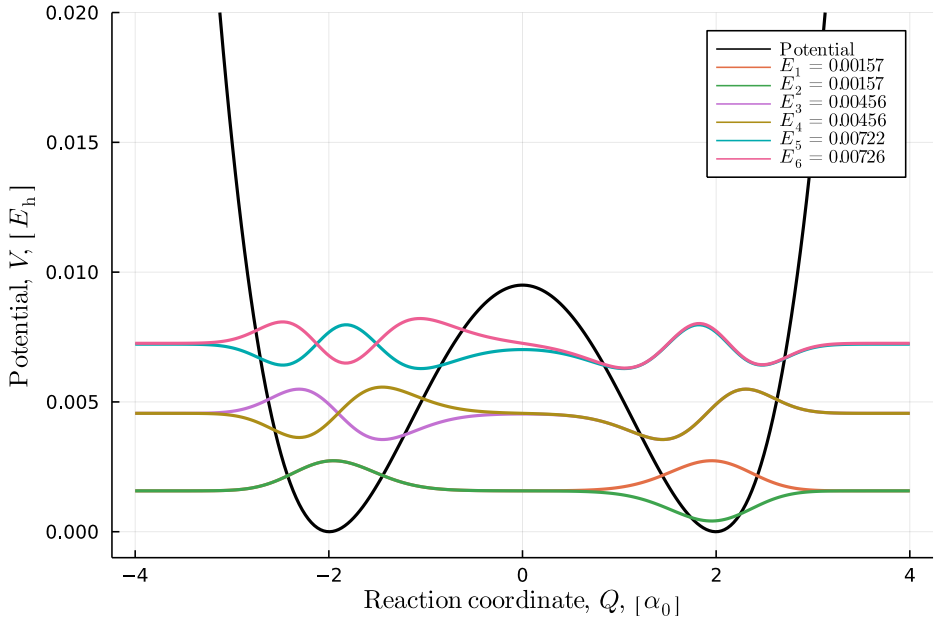

Supplementary Figure 10: The Topaler and Makri [17] DW1 benchmark potential, with the first 6 eigenstates shown.

of 0.62 which is less than half Craig's value of 1.54. The spike observed in (d) Supplementary Figure 11 does not appear in Craig's work. We believe that this is due to the difference between the exact methods to determine the rate. Regardless, the plateau value is similar to Craig, meaning that while we might have some large transient differences, we tend to similar values asymptotically.

Summing up, we find good overall agreement between the WM-CL approach and Craig's approach. Furthermore, our model can be extended to lower temperatures.

SUPPLEMENTARY NOTE 4: SENSITIVITY TO THE MASS AND THE KINETIC ISOTOPE EFFECT

Here we explore the model's sensitivity to the mass of the tunnelling particle. We vary the mass terms in the WM-CL equation and calculate how the rates and steady-state populations change. See the Methods section of the main paper.

In Supplementary Figure 12 we investigated the KIE against temperature. At low temperatures, the KIE rapidly increases, suggesting that the DPT becomes increasingly dependent on quantum contributions. Meanwhile, at high temperatures, the KIE exponentially tails off. At biological temperatures the KIE ~ 30. The KIE dependency on the temperature offers a somewhat different functional form than just the k_{QM}. As $T \to \infty$, the KIE tends to unity, suggesting that the quantum rate becomes mass-independent, matching the expected classical behaviour.

Supplementary Figure 13 demonstrates a strong dependence on the tautomeric occupation probability. At lower masses, the tautomeric occupation is high; however, as the mass increases, the occupation quickly drops off. Over the range of explored masses, the occupation varies by two orders of magnitude and is a purely quantum mechanical effect. This suggests that changing the mass significantly impacts quantum tunnelling.

SUPPLEMENTARY NOTE 5: SENSITIVITY TO THE REACTION BARRIER

More recent evidence has suggested that free energy interactions can provide a diverse range of energetic scenarios [23], suggesting that an ensemble of possible potentials can explain the proton transfer process. Therefore, exploring a sensitivity analysis of the potential energy surface on the proton transfer reaction would be of general interest. However, this would require significant further work using ensemble multi-scale modelling combined with a correction for tunnelling. We perform an isolated sensitivity analysis on the forward reaction barrier by introducing a simple modifying function. In order to investigate how the potential barrier influences the quantum-to-classical rate, we

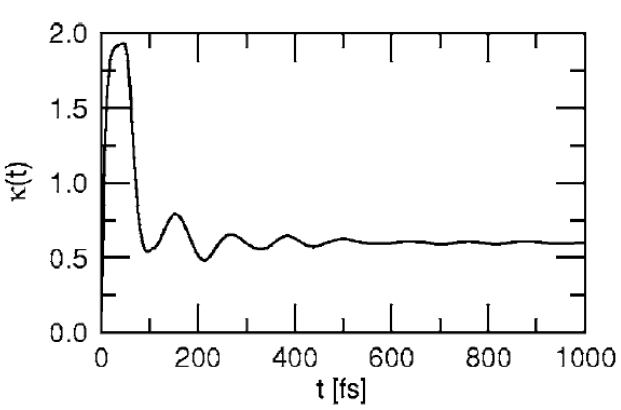

(a) Craig $\gamma = 0.05\,\omega_b$

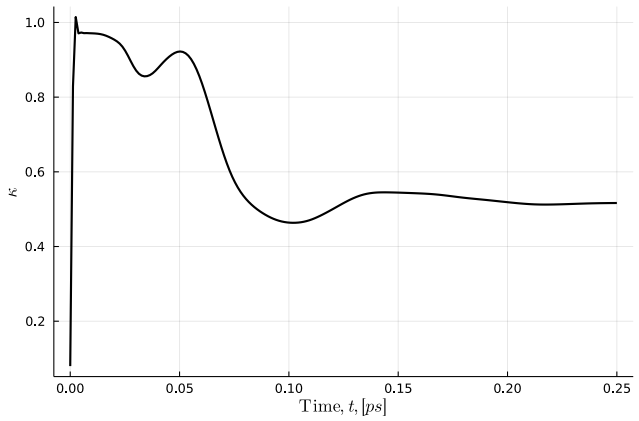

(b) WM-CL $\gamma = 0.05\,\omega_b$

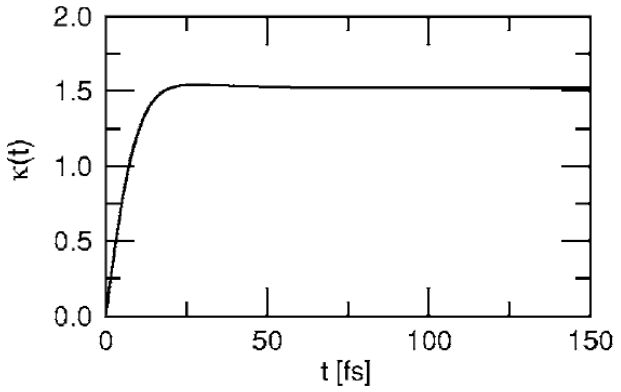

(c) Craig $\gamma = 0.95\,\omega_b$

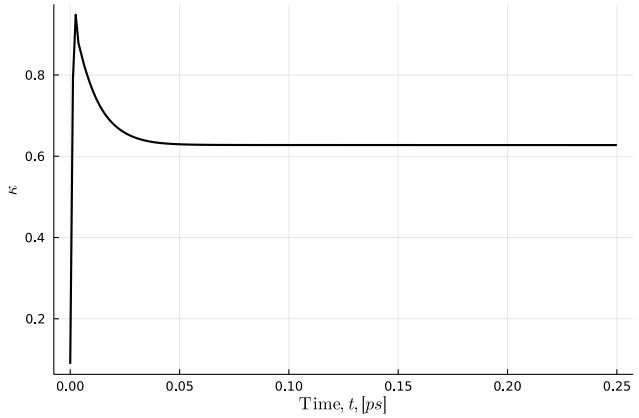

(d) WM-CL $\gamma = 0.95\,\omega_b$

Supplementary Figure 11: Comparing the numerical result of solving the WM-CL equation (right) with the DW1 model potential to the result of Craig *et al.* [18] (left). Reprinted from Craig *et al.* [18], with the permission of AIP Publishing.

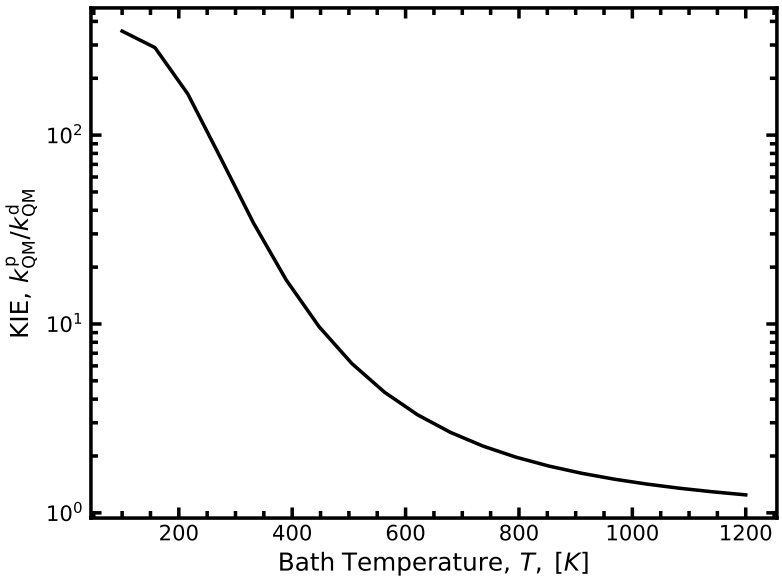

Supplementary Figure 12: Investigating the kinetic isotope effect for a range of temperatures.

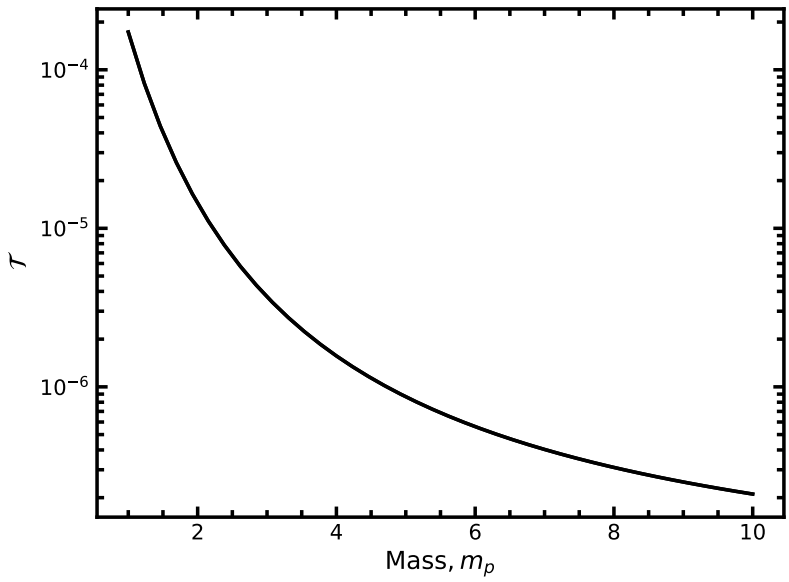

Supplementary Figure 13: Comparing the sensitivity of the tautomeric occupation probability as a function of the tunnelling mass.

conduct a sensitivity analysis on the barrier height. We change the potential by introducing a simple, smoothly varying Gaussian function,

$$f(q) = a \exp\left(-\frac{(q-b)^2}{2c^2}\right) + d. \tag{30}$$

Where a is the strength of the applied modification, b is the position of the centre of the peak, c is the standard deviation, and d vertically shifts the distribution. Applying the change to the potential using

$$V_{\mathrm{mod}}(q) = f(q) \cdot V(q). \tag{31}$$

The modified potential $V_{\mathrm{mod}}(q)$ is then inserted into our system Hamiltonian. We take $d = 1$ so that the peak modifies by strength a within the width interval c and leaves the rest of the potential unchanged. We set b to the location of the barrier so that only the barrier is modified. A width value of $c = 0.5\, a_0$ is sufficiently wide to modify as much of the barrier as possible while leaving the reaction asymmetry unchanged.

In Supplementary Figure 14 we vary the barrier height by up to 50% of the original value and observe how the dynamics and the steady-state populations change.

The classical rate demonstrates a linear dependence in logspace as a function of the reaction barrier height. As the barrier increases, the classical reaction rate swiftly drops. Over the range of barrier heights explored, the rate drops by over six orders of magnitudes. In contrast, the quantum rate is much higher than the classical rate over the entire range of barrier heights. Furthermore, the quantum rate exhibits a much shallower decline with increasing barrier height compared to the classical rate. Consequently, the quantum-to-classical rate shown in the middle panel is dominated by the quantum term, and since the quantum rate drops off at a slower rate, the quantum rate increasingly dominates at more considerable reaction barriers.

On the other hand, the tautomeric occupation probability changes by less than 10% of its value over the range of barrier heights explored. Here, the change in tautomeric occupation probability is more likely due to the modifying function amplifying the skew of the barrier. Since the canonical well is much more prominent in width, the barrier tail is much shorter on the tautomeric side, leading to a widening of the canonical well as a function of increasing barrier height, thus a decrease in tautomeric occupation probability.

In summary, we determine that increasing the barrier height significantly impacts the dynamics; namely, it causes a striking reduction in classical rate and affects the tunnelling much less. As a result, if the proton transfer barrier were to be much larger, we would see an increase in the quantum-to-classical contribution to the rate. Nevertheless, the conclusion would still stand; the rates are so high that the equilibrium populations of the canonical and tautomeric forms would quickly be reached.

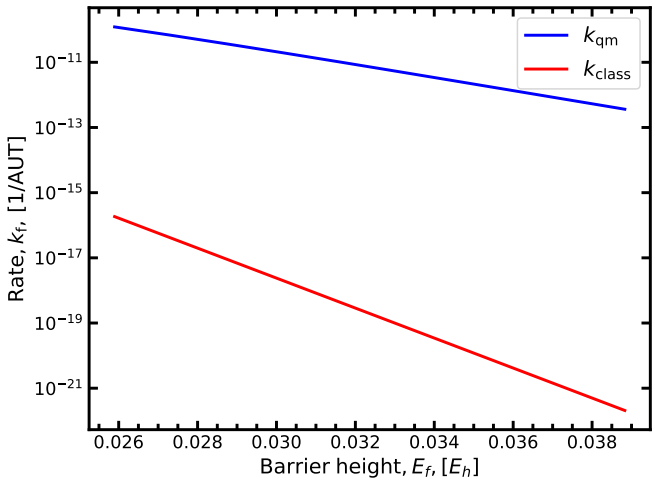

(a) Comparing the quantum and classical contributions to the reaction rates

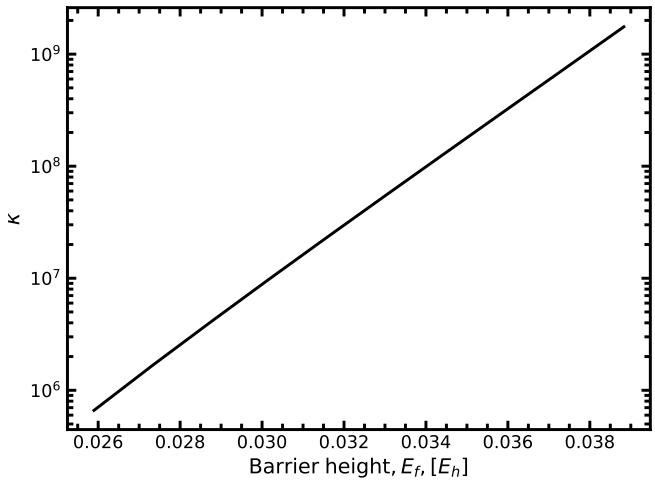

(b) The quantum-to-classical ratio

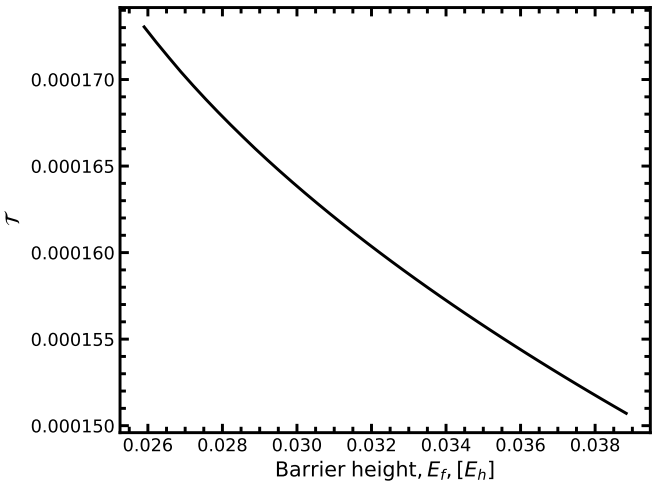

(c) Tautomeric occupation probability

Supplementary Figure 14: Comparing the sensitivity of the quantum and classical rates and the tautomeric occupation probability as a function of the forward reaction barrier. See text for details on the modifying function inducing the change in the reaction barrier.

SUPPLEMENTARY REFERENCES

[1] E. Wigner, On the quantum correction for thermodynamic equilibrium, Phys. Rev. **40**, 749 (1932).
[2] J. Weinbub and D. K. Ferry, Recent advances in wigner function approaches, Applied Physics Reviews **5**, 041104 (2018), https://doi.org/10.1063/1.5046663.
[3] J. E. Moyal, Quantum mechanics as a statistical theory, Mathematical Proceedings of the Cambridge Philosophical Society **45**, 99–124 (1949).
[4] K. İmre, E. Özizmir, M. Rosenbaum, and P. F. Zweifel, Wigner method in quantum statistical mechanics, Journal of Mathematical Physics **8**, 1097 (1967), https://doi.org/10.1063/1.1705323.
[5] A. O. Caldeira and A. J. Leggett, Path integral approach to quantum brownian motion, Physica A: Statistical mechanics and its Applications **121**, 587 (1983).
[6] C. Trahan and R. Wyatt, *Quantum Dynamics with Trajectories: Introduction to Quantum Hydrodynamics*, Interdisciplinary Applied Mathematics (Springer New York, 2006).
[7] W. H. Zurek, Preferred States, Predictability, Classicality and the Environment-Induced Decoherence, Progress of Theoretical Physics **89**, 281 (1993), https://academic.oup.com/ptp/article-pdf/89/2/281/5226677/89-2-281.pdf.
[8] R. Cabrera, D. I. Bondar, K. Jacobs, and H. A. Rabitz, Efficient method to generate time evolution of the wigner function for open quantum systems, Physical Review A **92**, 042122 (2015).
[9] I. Burghardt and K. B. Møller, Quantum dynamics for dissipative systems: A hydrodynamic perspective, The Journal of chemical physics **117**, 7409 (2002).
[10] G. Agarwal, Brownian motion of a quantum oscillator, Physical Review A **4**, 739 (1971).
[11] F. Haake and R. Reibold, Strong damping and low-temperature anomalies for the harmonic oscillator, Physical Review A **32**, 2462 (1985).
[12] F. Haake, H. Risken, C. Savage, and D. Walls, Master equation for a damped nonlinear oscillator, Physical Review A **34**, 3969 (1986).
[13] K. H. Hughes, Dissipative quantum phase space dynamics on dynamically adapting grids, The Journal of chemical physics **122**, 074106 (2005).
[14] Y. Tanimura and P. G. Wolynes, Quantum and classical fokker-planck equations for a gaussian-markovian noise bath, Phys. Rev. A **43**, 4131 (1991).
[15] A. Donoso and C. C. Martens, Solution of phase space diffusion equations using interacting trajectory ensembles, The Journal of chemical physics **116**, 10598 (2002).
[16] F. Grossmann and W. Koch, A finite-difference implementation of the caldeira–leggett master equation, The Journal of chemical physics **130**, 034105 (2009).
[17] M. Topaler and N. Makri, Quantum rates for a double well coupled to a dissipative bath: Accurate path integral results and comparison with approximate theories, The Journal of Chemical Physics **101**, 7500 (1994), https://doi.org/10.1063/1.468244.
[18] I. R. Craig, M. Thoss, and H. Wang, Proton transfer reactions in model condensed-phase environments: Accurate quantum dynamics using the multilayer multiconfiguration time-dependent hartree approach, The Journal of Chemical Physics **127**, 144503 (2007), https://doi.org/10.1063/1.2772265.
[19] A. Pomyalov and D. J. Tannor, The non-markovian quantum master equation in the collective-mode representation: Application to barrier crossing in the intermediate friction regime, The Journal of Chemical Physics **123**, 204111 (2005), https://doi.org/10.1063/1.2121649.
[20] T. Yamamoto, H. Wang, and W. H. Miller, Combining semiclassical time evolution and quantum boltzmann operator to evaluate reactive flux correlation function for thermal rate constants of complex systems, The Journal of Chemical Physics **116**, 7335 (2002), https://doi.org/10.1063/1.1464539.
[21] L. Chen and Q. Shi, Quantum rate dynamics for proton transfer reactions in condensed phase: The exact hierarchical equations of motion approach, The Journal of Chemical Physics **130**, 134505 (2009), https://doi.org/10.1063/1.3097128.
[22] I. R. Craig and D. E. Manolopoulos, Chemical reaction rates from ring polymer molecular dynamics, The Journal of Chemical Physics **122**, 084106 (2005), https://doi.org/10.1063/1.1850093.
[23] A. Gheorghiu, P. Coveney, and A. Arabi, The influence of base pair tautomerism on single point mutations in aqueous dna, Interface focus **10**, 20190120 (2020).